International Journal of Microwave and Wireless Technologies

cambridge.org/mrf

A novel planar balanced-to-balanced diplexer with high isolation and harmonic suppression

Changqing Geng, Zhongbao Wang, Dehao Zhao, Hongmei Liu and Shaojun Fang

School of Information Science and Technology, Dalian Maritime University, Dalian, LN, China

Research Paper

Cite this article: Geng C, Wang Z, Zhao D, Liu H, Fang S (2026) A novel planar balanced-to-balanced diplexer with high isolation and harmonic suppression. *International Journal of Microwave and Wireless Technologies* **18**(1), 46–55. https://doi.org/10.1017/S1759078726102955

Received: 12 June 2025
Revised: 24 January 2026
Accepted: 26 January 2026

Keywords:
balanced-to-balanced; diplexer; harmonic suppression; high isolation

Corresponding author: Zhongbao Wang; Email: wangzb@dlmu.edu.cn

Abstract

This paper presents a novel planar balanced-to-balanced diplexer with high isolation and harmonic suppression. Both the lower and higher channels of the diplexer consist of the two-stepped impedance resonators and one uniform impedance resonator. To enhance the inter-channel isolation of the diplexer, the cross-coupling between the resonators is used to introduce extra out-of-band transmission zeros. By utilizing stepped impedance resonators with different impedance ratios, the harmonics of the three resonators, except the fundamental harmonics, are different from each other so as to suppress the odd- and even-mode harmonics effectively and ultimately to achieve the purpose of broadening the stopband and enhancing the common-mode (CM) suppression. To verify the feasibility of this design, a microstrip prototype with dual-channel center frequencies of 2.01 GHz and 3.54 GHz was manufactured. Experimental results demonstrate that the in-band differential-mode (DM) isolation is higher than 41.6 dB and 41.5 dB for the lower and higher channels, respectively. CM suppression is greater than 20 dB in the 0–13.7 GHz range for the lower channel and 20 dB in the 0–9.0 GHz range for the higher channel. The stopband suppression level achieves 20 dB up to 18.5 GHz.

Introduction

Diplexers are essential passive components in microwave systems, which can work together with antennas to transmit and receive required signals [1–3]. However, with the rapid advancements in wireless communication systems, diplexers are now needed to meet more rigorous requirements. Traditionally, the widely adopted approach involves connecting two bandpass filters with different center frequencies using a T-junction [4, 5]. But this method necessitates additional matching circuits, resulting in an oversized circuit size. Therefore, researchers have explored alternative designs to reduce circuit size; many diplexers with compact sizes were published in refs [6–9]. But their inter-channel isolation is poor. To address this issue, the isolation is improved while realizing a compact structure by sharing a resonator as the filtering structure and feeding network to increase the out-of-band transmission zeros in refs [10–12]. However, the above diplexers are single-ended structures and cannot provide high immunity to electromagnetic interference and noise [13, 14]. Therefore, many unbalanced-to-balanced diplexers have been proposed [15–17], but this design is not suitable for use in systems with differential antennas and is insufficient to cope with the complex and variable noise environment [18]. As shown in Fig. 1, balanced-to-balanced diplexers are particularly important in high-density communication environments as critical interface devices between differential antennas and differential transceivers in the radio-frequency (RF) front end [19, 20]. In recent years, balanced-to-balanced diplexer designs utilizing symmetrical resonators or microstrip-to-slotline transition structures have been published in refs [21–24]. However, the balanced-to-balanced diplexer in Zhang et al. [21] has insufficient in-band common-mode (CM) noise suppression (only 23 dB). Besides, the 20-dB bandwidths of differential-mode (DM) stopband [22–24] and out-of-band CM noise suppression [22, 23] are narrow. Accordingly, the harmonics are made to move away from the passband by exploiting the harmonic characteristics of the resonator [25–27], thus broadening 20-dB bandwidths of the DM stopband and the CM noise suppression. But the bandwidths of the DM stopband and the CM noise suppression broadened in this way are often limited by the structure of resonators and cannot realize a more excellent wide DM stopband response and a wideband CM noise suppression response.

To overcome these issues, this paper has proposed a novel planar balanced-to-balanced diplexer with high isolation and harmonic suppression, which is designed and fabricated on the F4B substrate with $h = 1.0$ mm, $\varepsilon_r = 2.6$, and $\tan\delta = 0.003$. The filtering structure of the proposed diplexer comprises two-stepped impedance resonators (SIRs) and one uniform impedance resonator (UIR). The differential feed ports symmetrically excite the SIR for CM suppression and DM transmission. In order to enhance the inter-channel isolation of the diplexer,

© The Author(s), 2026. Published by Cambridge University Press in association with The European Microwave Association.

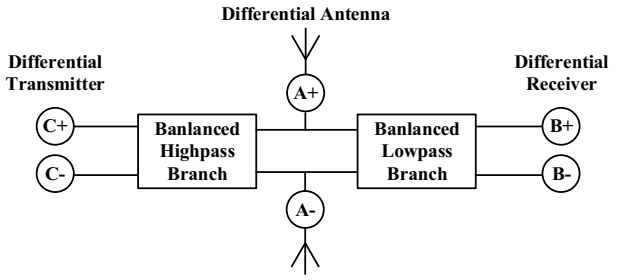


Figure 1. The structure of the RF front-end with a balanced-to-balanced diplexer.

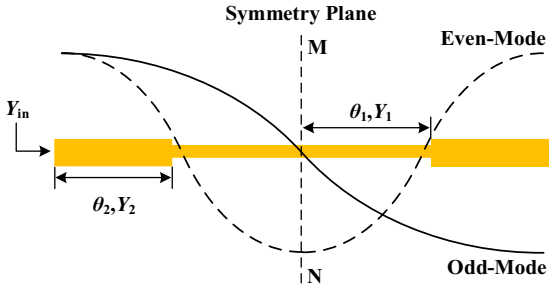


Figure 2. The structure of the stepped impedance resonator.

the cross-coupling between the SIRs is used to introduce the extra out-of-band transmission zeros. At the same time, the harmonic characteristics of SIRs with different impedance ratios are utilized so that the harmonics of each channel are suppressed by the asymmetric configuration of SIRs, which cannot form an effective spurious passband, thereby broadening the DM stopband and enhancing the out-of-band CM suppression. Specifically, the contribution of this work can be summarized as follows: (i) excellent harmonic suppression (wide DM stopband and wideband CM suppression), (ii) excellent DM isolation, and (iii) great design flexibility. The detailed design methodology is described as follows.

Diplexer structure and analysis

Characteristics of the SIR and UIR

Based on the selected F4B substrate, this section begins by introducing the SIR and UIR. The structure of the SIR is depicted in Fig. 2, where θ_i and Y_i (i = 1, 2) represent the electrical length and characteristic admittance of the microstrip line, respectively. According to transmission line theory, the input admittance of SIR is

$$Y_{in} = \frac{2jY_2(R_z \tan\theta_1 + \tan\theta_2)(R_z - \tan\theta_1 \tan\theta_2)}{R_z(1-\tan^2\theta_1)(1-\tan^2\theta_2) - 2(1-R_z^2)\tan\theta_1 \tan\theta_2} \quad (1)$$

where R_z is the impedance ratio, $R_z = Y_1/Y_2$. When $R_z = 1$, it is UIR. When $Y_{in} = 0$, the odd- and even-mode resonance conditions can be derived as

$$\tan[(1-a)(\theta_1+\theta_2)]\tan[\alpha(\theta_1+\theta_2)] = R_2 \quad (\text{Odd}-\text{mode}) \quad (2)$$

$$R_z tan[(1-\alpha)(\theta_1+\theta_2)] + \tan[a(\theta_1+\theta_2)] = 0 \quad (\text{Evee}-\text{mode}) \quad (3)$$

where α is the electrical length ratio, $\alpha = \theta_2/(\theta_1 + \theta_2)$. From Equations (2) and (3), it can be analyzed that for the SIR, both the odd- and even-mode resonance conditions are related to θ_i, α, and R_z. As illustrated in Fig. 2, the solid and dashed lines indicate

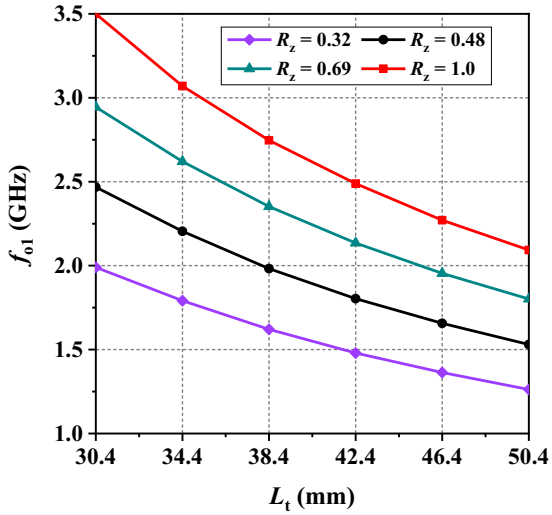


Figure 3. Curves of the variation of f_{o1} with the physical dimension L_t (Y_1 = 0.0114 S).

the voltage distribution of the SIR under odd- and even-mode excitation, respectively, and the symmetry plane MN behaves as a shorted circuit under odd-mode excitation and an opened circuit under even-mode excitation, which ensures that the dominant resonance is excited exclusively by the DM signal and effectively suppresses the CM noise.

The SIR has an infinite number of resonant modes. The fundamental resonance occurs in the odd-mode, the second resonance in the even-mode, and higher-order resonances in that order. Here we discuss the first five resonance modes in detail. Figure 3 plots the variation of the f_{o1} (the first-order odd-mode resonant frequency of the SIR) with the physical dimension L_t (L_t is the total physical length corresponding to the electrical length $2\theta_1 + 2\theta_2$) when R_z is different. The results indicate that f_{o1} gradually decreases as L_t increases, and when f_{o1} is identical, the overall physical dimension decreases as the R_z decreases. Accordingly, the stepped impedance structure facilitates a compact design [6, 7]. Figure 4 depicts the variation of the resonant frequencies ratio with α when R_z is different; it suggests that when $R_z < 1$, with the increase of α, the f_{e1}/f_{o1} increases gradually, the f_{o2}/f_{o1} and f_{e2}/f_{o1} initially increase and then decrease, and the f_{o3}/f_{o1} first increases, then decreases, and then increases again. Here, f_{e1} represents the first-order even-mode resonant frequency of the SIR, f_{o2} represents the second-order odd-mode resonant frequency of the SIR, f_{e2} represents the second-order even-mode resonant frequency of the SIR, and f_{o3} represents the third-order odd-mode resonant frequency of the SIR. And these high-order resonant frequencies increase as R_z decreases, as shown in Fig. 4. That is to say, by adjusting the R_z and α, the higher-order harmonics of SIRs can be positioned at different locations, which indicates that SIRs with different R_z and α will contribute to achieving wide DM stopband and wideband CM suppression. Besides, this design does not require tuning the resonant frequency ratio to its maximum; it only needs to ensure that the spurious harmonics of the used resonators are as widely spaced as possible. Through experimental verification, from the point of view of suppressing spurious harmonics and achieving a compact layout, the R_z of the SIRs are ultimately selected as 0.69 and 0.32 for the lower channel, and the R_z of the SIRs are ultimately selected as 0.69 and 0.48 for the higher channel. To simplify the simulation, the α for SIR with R_z = 0.69 is set to 0.51, while the α for R_z = 0.32 and R_z = 0.48 are both set to 0.43.

https://doi.org/10.1017/S1759078726102955 Published online by Cambridge University Press

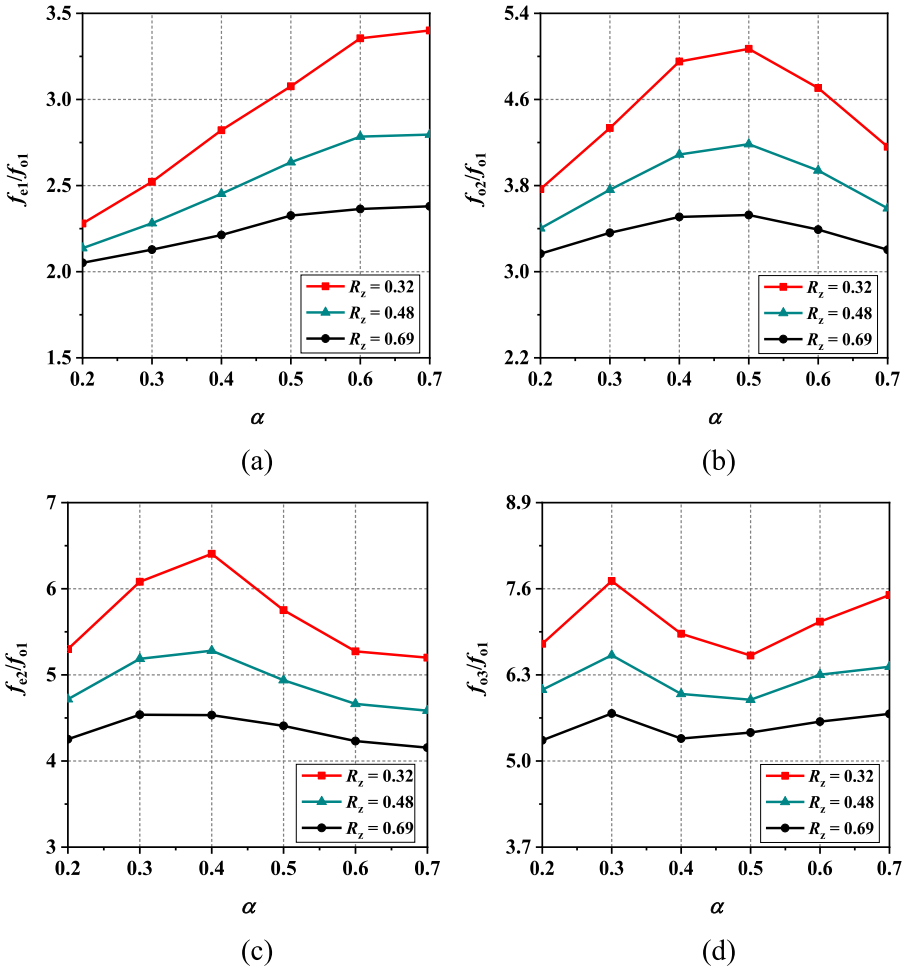


Figure 4. Curves of the variation of the resonant frequencies ratio with the α ($Y_1 = 0.0114$ S). (a) f_{e1}/f_{o1}, (b) f_{o2}/f_{o1}, (c) f_{e2}/f_{o1}, (d) f_{o3}/f_{o1}.

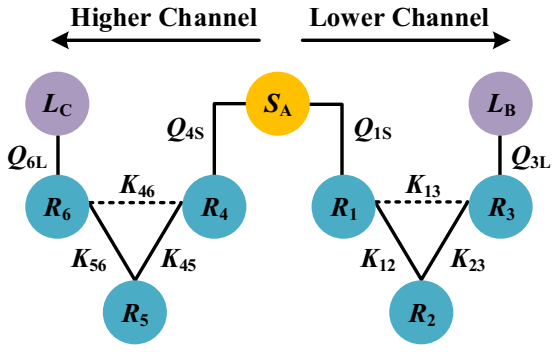


Figure 5. The coupling topology of the proposed balanced diplexer.

Coupling routing scheme

Figure 5 illustrates the coupling topology of the proposed balanced diplexer. In this topology, S and L represent the differential source and load, respectively; solid lines denote strong coupling, dashed lines denote weak coupling, R_1, R_3, R_4, and R_6 correspond to fundamental resonant modes of the SIRs, and R_2 and R_5 denote fundamental resonant modes of the UIRs. Their resonant frequencies are f_{R1}, f_{R3}, f_{R4}, f_{R6}, f_{R2}, and f_{R5}.

The lower channel is formed by coupling the three resonators R_1, R_2, and R_3, while the higher channel is established by coupling R_4, R_5, and R_6. Both channels exhibit a third-order bandpass response, enhancing channel selectivity. DM isolation between channels is improved by introducing out-of-band transmission zeros through cross-coupling between SIRs. And by adjusting K_{13} and K_{46}, the transmission zeros can be controlled. Here, the control of the transmission zero of the lower channel is described as an example. The control mechanism of the transmission zero of the higher channel is similar to it. Figure 6 illustrates the curve of the transmission coefficients with the different values of K_{13}. It can be observed that as the coupling coefficient K_{13} gradually increases, the transmission zero gradually moves closer to the passband, but the stopband suppression level deteriorates. Therefore, when adjusting the transmission zero, it is necessary to weigh the suppression level of the stopband, ultimately selecting an appropriate coupling coefficient K_{13}. It is also worth noting that the lower and higher channels each possess independent transmission paths, allowing for separate control over the center frequencies and bandwidths. This ensures that the design of the balanced diplexer has greater flexibility.

Design of the balanced-to-balanced diplexer

The evolution of the bandpass filtering structures is shown in Fig. 7. Both structures use cross-coupling to introduce additional transmission zeros. For structure 1 with a symmetric configuration

https://doi.org/10.1017/S1759078726102955 Published online by Cambridge University Press

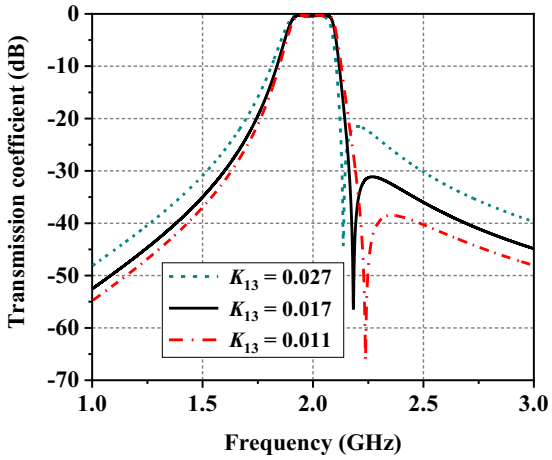


Figure 6. Curve of the transmission coefficients with the different K_{13}.

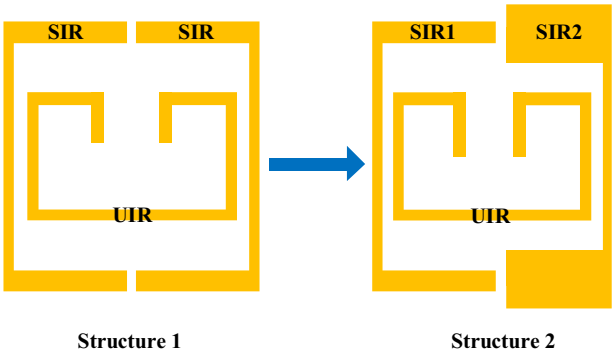


Figure 7. The evolution of the bandpass filtering structures.

of SIRs, although an upper stopband up to $3.5f_0$ and CM suppression up to $2.3f_0$ are achieved by adjusting the impedance ratio of the SIRs to keep their second-order odd-mode and first-order even-mode harmonics away from the fundamental resonance frequency f_0, they still affect the performance of the diplexer through the weak coupling path. For structure 2 with an asymmetric configuration of SIRs, in order to further broaden the upper stopband and CM suppression bandwidths, employ SIRs with different impedance ratios, such that the harmonics of the two SIRs and UIR are different from each other. When the passband center frequency is 2.0 GHz, the resonant-frequency spectra of SIR1, SIR2, and UIR are shown in Fig. 8, which shows that, except for the fundamental frequencies (i.e., first-order odd-mode resonances), the three resonators have different first-order even-mode harmonics, second-order odd-mode harmonics, second-order even-mode harmonics, third-order odd-mode harmonics, etc.

The balanced diplexer is designed with the layout shown in Fig. 9. Port A serves as the differential antenna port, while Ports B and C function as the differential transceiver port. The transmission coefficients between the differential ports can be defined by the mixed-mode *S*-parameters [28]. For example, the DM and CM transmission coefficients between differential Port A and differential Port B can be defined as $|S_{ddBA}|$ and $|S_{ccBA}|$, respectively, which represent the transmission responses between differential ports.

Compared to the parallel-coupled single-band and dual-band bandpass filters using the SIRs with different dimensions [29, 30], the coupling topology and the input/output feed method of the

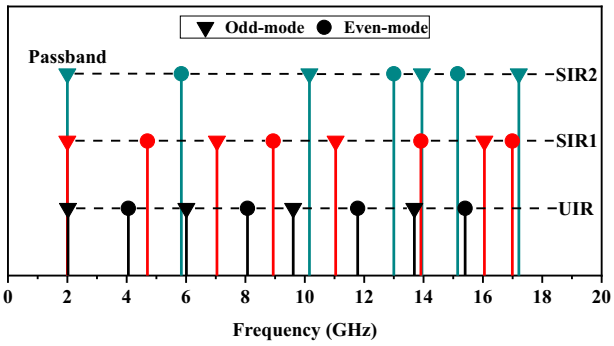


Figure 8. The resonant-frequency spectra of SIRs and UIR.

filtering structures in this paper and the principle of harmonic suppression are different. The principle of harmonic suppression in Kuo and Lin [30] is to collocate the transmission zeros generated by the tap feed method [29] and inherent transmission zeros of open-circuited parallel-coupled lines [30], but the principle of harmonic suppression in this paper is based on the excitation principle. Specifically, based on the layout and coupling topology of the proposed balanced diplexer shown in Fig. 9 and Fig. 5, due to the symmetrical feed ports exciting the SIRs, the even- and odd-mode harmonics of the SIRs only can be excited by common- and differential-modes, respectively; thus, the DM signal can pass only when the three resonators (SIR1, SIR2, and UIR) have the same odd-mode resonant frequency, and when the odd-mode resonant frequencies of the three resonators are different, especially when the odd-mode resonant frequencies of resonators R_1 and R_3 are different, the DM signal will be blocked to achieve a wide DM stopband. Similarly, when the even-mode resonant frequencies of resonators R_1 and R_3 are different, the CM noise will also be blocked to achieve wideband CM suppression. In this design, the three resonators have the same resonant frequency only at the fundamental frequency, while the even- and odd-mode spurious harmonics of the three resonators cannot resonate at the same frequency in the high-frequency band. Therefore, the proposed diplexer can result in wideband harmonic suppression. For example, between differential Port A and differential Port B, the comparison of the DM upper stopband (which can be expressed by $|S_{ddBA}|$) and CM suppression (which can be expressed by $|S_{ccBA}|$) simulation results for two different filtering structures is shown in Fig. 10.

It can be seen from Fig. 10(a) that for the structure 1 (resonators R_1 and R_3 use the same SIR1, the second-order and third-order odd-mode harmonics of which resonate at about 7.1 GHz and 11 GHz, respectively, as shown in Fig. 8), the DM out-of-band suppression near 7.1 GHz and 11 GHz is only about 12 dB (i.e., $|S_{ddBA}|$ is about − 12 dB), but when resonators R_1 and R_3 use the different SIRs (i.e., the structure 2 with asymmetric configuration of SIRs), resonators R_1 and R_3 (i.e., SIR1 and SIR2) have different resonant frequencies of second-order and third-order odd-mode harmonics, the DM out-of-band suppression near 7.1 GHz and 11 GHz has been significantly enhanced, achieving a wide 20-dB DM stopband. It can be seen from Fig. 8 that the first-order and second-order even-mode harmonics of the SIR1 resonate at about 4.7 GHz and 9 GHz, respectively; thus, the CM suppression for the structure 1 near 4.7 GHz and 9 GHz is less than 20 dB (i.e., $|S_{ccBA}| > -20$ dB), as shown in Fig. 10(b). Similarly, by using an asymmetric configuration of SIRs, different even-mode resonant

https://doi.org/10.1017/S1759078726102955 Published online by Cambridge University Press

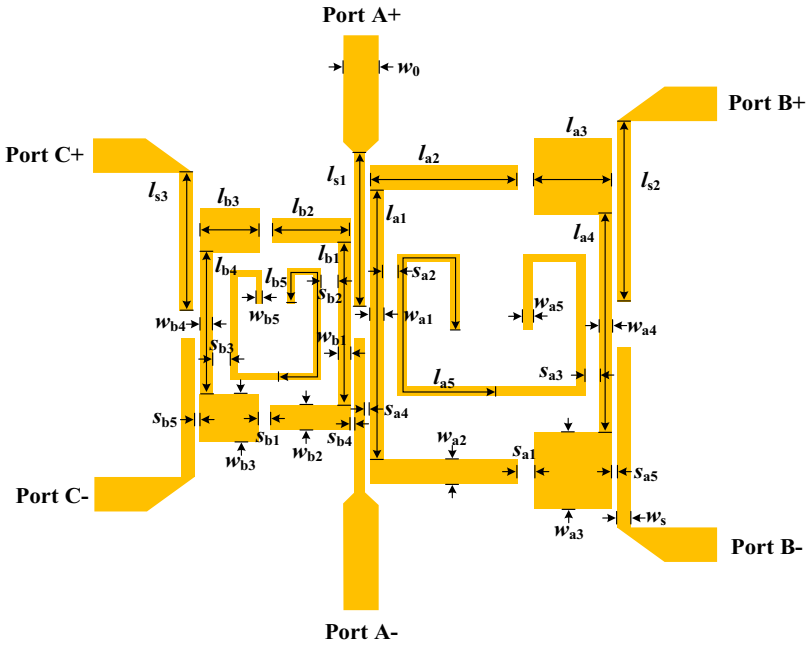


Figure 9. Layout of the proposed balanced diplexer.

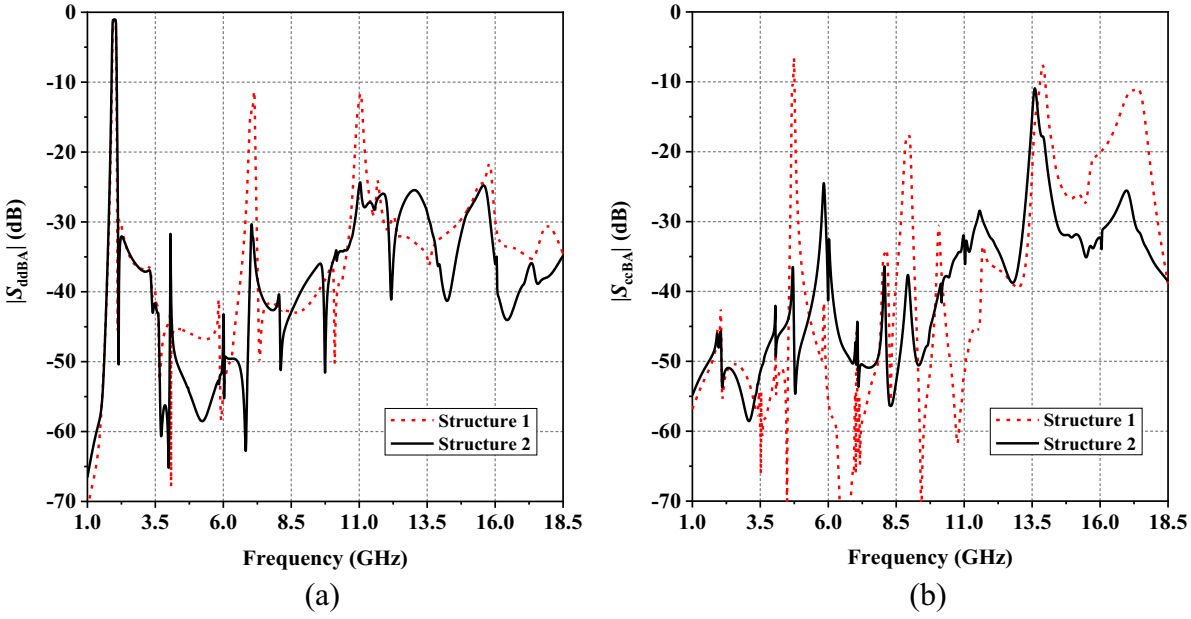


Figure 10. The comparison of the stopband and CM suppression simulation results. (a) $|S_{ddBA}|$, (b) $|S_{ccBA}|$.

frequencies of SIR1 and SIR2 result in 20-dB CM suppression up to 13.4 GHz, achieving wideband CM suppression.

The design specifications for the lower channel of the balanced diplexer are as follows: The center frequency f_L is 2.0 GHz with a 3-dB fractional bandwidth (FBW) of 7.5% and a return loss (RL) of 15 dB. The coupling matrix can be synthesized as

$$\mathbf{M_L} = \begin{bmatrix} 0 & 0.794 & 0 & 0 & 0 \\ 0.794 & 0 & 0.647 & 0.227 & 0 \\ 0 & 0.647 & -0.285 & 0.720 & 0 \\ 0 & 0.227 & 0.720 & 0 & 0.959 \\ 0 & 0 & 0 & 0.959 & 0 \end{bmatrix} \quad (4)$$

The required coupling coefficients K_{12}, K_{13}, and K_{23} and the lower channel loaded quality factors (Loaded-Q) Q_{1S} and Q_{3L} are calculated as [31]:

$$K_{12} = \text{FBW} \cdot m_{12},\ K_{13} = \text{FBW} \cdot m_{13},\ K_{23} = \text{FBW} \cdot m_{23} \quad (5)$$

$$Q_{1S} = \frac{1}{\text{FBW} \cdot m_{1S}^2},\ Q_{3L} = \frac{1}{\text{FBW} \cdot m_{3L}^2} \quad (6)$$

The required fundamental resonant frequency of the UIR is determined by the following equation [31]:

$$f_{R2} = f_L \cdot \left(1 - \frac{m_{22} \cdot \text{FBW}}{2}\right) \quad (7)$$

https://doi.org/10.1017/S1759078726102955 Published online by Cambridge University Press

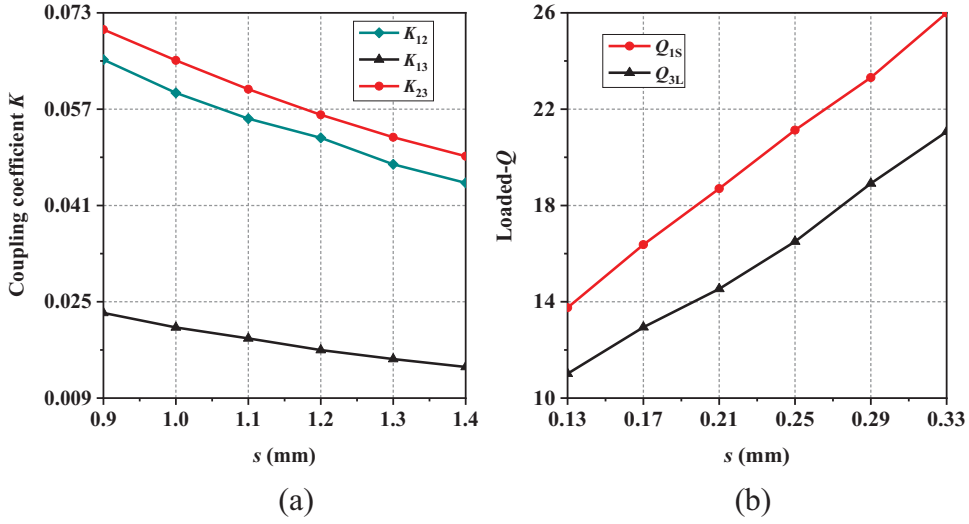


Figure 11. The curves of coupling coefficients K and loaded-Q for the lower channel as the gap s changes. (a) Coupling coefficients K. (b) Loaded-Q.

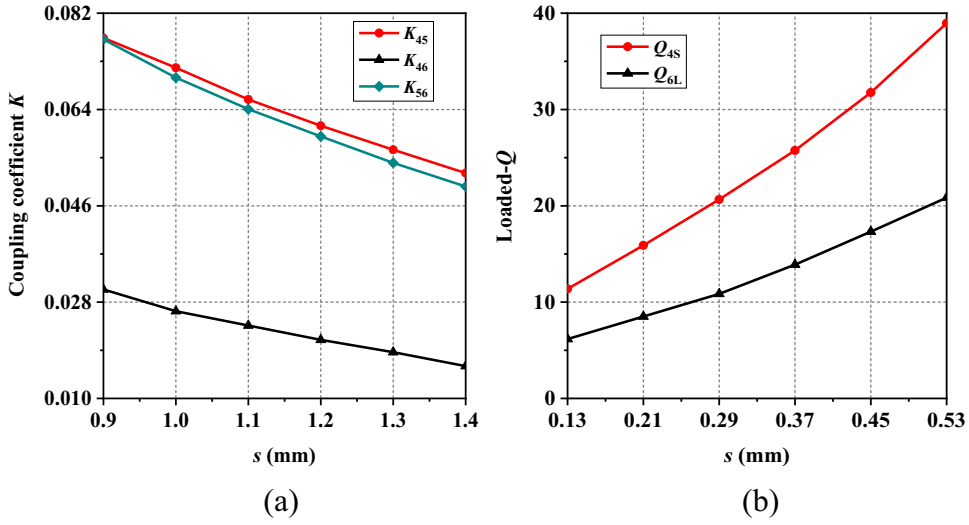


Figure 12. The curves of coupling coefficients K and loaded-Q for the higher channel as the gap s changes. (a) Coupling coefficients K. (b) Loaded-Q.

$$\mathbf{M_H} = \begin{bmatrix} 0 & 0.887 & 0 & 0 & 0 \\ 0.887 & 0 & 0.650 & 0.350 & 0 \\ 0 & 0.650 & -0.445 & 0.625 & 0 \\ 0 & 0.350 & 0.625 & 0 & 0.829 \\ 0 & 0 & 0 & 0.829 & 0 \end{bmatrix} \quad (8)$$

Based on Equations (5)–(7), the calculated parameters for the lower channel are $K_{12} = 0.0485$, $K_{13} = 0.0170$, $K_{23} = 0.0540$, $Q_{1S} = 21.15$, $Q_{3L} = 14.50$, $f_{R1} = f_{R3} = 2000.0$ MHz, and $f_{R2} = 2021.4$ MHz. Figure 11(a) shows the curves of coupling coefficients K for the lower channel as the gap s changes. Figure 11(b) illustrates the curves of loaded-Q as the gap s changes. To meet the design specifications, the coupling coefficients K and the loaded-Q must match the calculated values. This can be achieved by carefully selecting the relevant physical dimensions, as indicated in Fig. 11, to satisfy the design requirements. And the resonant frequencies of the resonators are adjusted by tuning length.

The center frequency f_H, 3-dB FBW, and RL of the higher channel of the balanced diplexer are 3.5 GHz, 8.0%, and 15 dB, respectively, with the coupling matrix given by Equation (8). Similarly, the required coupling coefficients K, loaded-Q, and fundamental resonant frequencies are calculated as follows: $K_{45} = 0.0520$, $K_{46} = 0.0280$, $K_{56} = 0.0500$, $Q_{4S} = 15.89$, $Q_{6L} = 18.19$, $f_{R4} = f_{R6} = 3500.0$ MHz, and $f_{R5} = 3562.3$ MHz. Figure 12(a) illustrates the curves of the higher channel coupling coefficients K as the gap s changes. Figure 12(b) shows the relationship between the higher channel loaded-Q and the gap s. By carefully selecting the relevant physical dimensions based on Fig. 12, the desired coupling coefficients K and loaded-Q can be achieved to meet the design specifications. And the self-resonant frequencies are adjusted by tuning length.

Design procedure

Based on the above analysis, the design procedure for the proposed novel planar balanced-to-balanced diplexer with high isolation and harmonic suppression can be summarized as follows:

https://doi.org/10.1017/S1759078726102955 Published online by Cambridge University Press

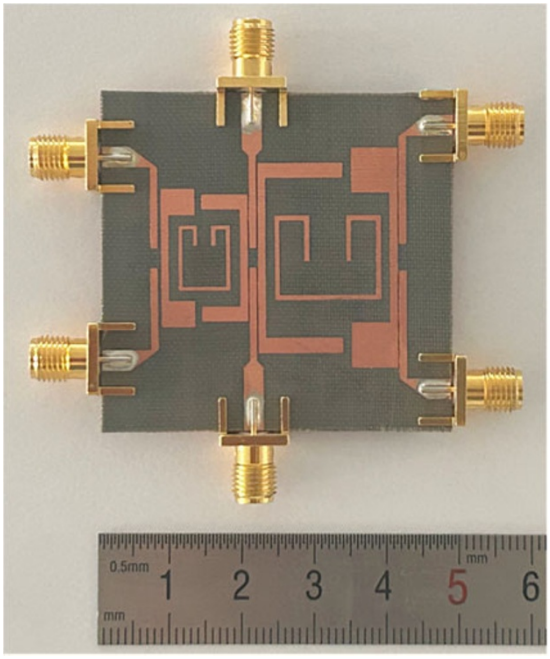


Figure 13. The photograph of the fabricated prototype.

Step 1: Define diplexer center frequencies, along with the 3-dB FBW and RL, and synthesize the coupling matrix.

Step 2: Using the synthesized coupling matrix, determine the center frequencies of the SIRs and the UIR, and employ eigenmode analysis in HFSS to select the appropriate impedance ratio for the SIRs and sequentially simulate the different gaps according to coupling coefficients K and the loaded-Q. Ensure that both channels exhibit great third-order filtering responses.

Step 3: Combine the two channel structures and perform simulations. Optimize the physical dimensions of the overall structure to address potential issues arising from the discontinuity and the interaction.

Experimental verification

The proposed novel planar balanced-to-balanced diplexer, featuring high isolation and harmonic suppression, is designed and fabricated on the F4B substrate. A photograph of the fabricated prototype is shown in Fig. 13. The overall circuit size is $0.47\lambda_g \times 0.44\lambda_g$ (48 mm × 45 mm), where λ_g is the guided wavelength at f_L. The optimized final physical dimensions of the proposed balanced diplexer are shown in Table 1 (unit: mm). The simulated and measured results are presented in Fig. 14. The various mixed S-parameters are defined as follows: $|S_{ddAA}|$ represents the reflection coefficients under DM excitation, $|S_{ddBA}|$ and $|S_{ddCA}|$ represent the transmission coefficients under DM excitation, $|S_{ccBA}|$ and $|S_{ccCA}|$ represent the transmission coefficients under CM excitation, $|S_{ddBC}|$ represents DM isolation, and $|S_{ccBC}|$ represents CM isolation.

As shown in Fig. 14(a) and 14(b), the measured center frequencies for the lower and higher channels are 2.01 GHz and 3.54 GHz, respectively. The corresponding in-band minimum insertion losses are 1.55 dB and 1.81 dB, while the 3-dB FBWs are 7.4% and 8.1%. Transmission zeros near the passband are observed at 2.17 GHz and 3.73 GHz. It is also worth mentioning that 20-dB out-of-band suppression is achieved up to 18.5 GHz ($9.2f_L$), featuring wide upper stopband responses. As depicted in Fig. 14(c) and 14(d), the in-band DM isolation exceeds 41.6 dB and 41.5 dB for the lower and higher channels, respectively. In the range of 0-18.5 GHz, the DM isolation exceeds 23.0 dB, while the CM isolation is better than 27.4 dB. As plotted in Fig. 14(e) and 14(f), the in-band CM suppression is greater than 44.1 dB and 39.6 dB for the lower and higher channels, respectively. Lower-channel CM suppression is better than 20 dB in the 0–13.7 GHz ($6.8f_L$) range, and higher-channel CM suppression is better than 20 dB in the 0–9.0 GHz ($2.54f_H$) range. The discrepancy between simulated and measured results is mainly due to the fabrication tolerances, the substrate characteristic instability, and the impedance mismatch between the SMA connectors and the PCB circuit at high frequencies.

Table 2 provides performance comparisons with previous works. As shown in Table 2, the proposed balanced diplexer exhibits a wide stopband and excellent CM suppression, which indicates that it has strong immunity to noise interference. Furthermore, the high DM isolation significantly reduces interchannel crosstalk.

Conclusion

In this paper, a novel planar balanced-to-balanced diplexer with high isolation and harmonic suppression, designed using SIRs and UIR, is presented. While utilizing cross-coupling between SIRs to introduce transmission zeros, the impedance ratio of SIRs is flexibly adjusted to effectively suppress harmonics. Moreover, the theory and design methodology for the proposed diplexer are

Table 1. The optimized final dimensions of the proposed balanced diplexer (unit: mm)

l_{s1}	l_{s2}	l_{s3}	l_{a1}	l_{a2}	l_{a3}	l_{a4}
12.4	14.4	10.85	21.4	11.6	6.31	17.4
l_{a5}	l_{b1}	l_{b2}	l_{b3}	l_{b4}	l_{b5}	w_0
27.08	13.0	6.27	4.58	11.5	15.11	2.76
w_s	w_{a1}	w_{a2}	w_{a3}	w_{a4}	w_{a5}	w_{b1}
1.0	1.0	2.0	6.0	1.0	0.65	1.0
w_{b2}	w_{b3}	w_{b4}	w_{b5}	s_{a1}	s_{a2}	s_{a3}
2.0	3.5	1.0	0.5	1.2	1.26	1.26
s_{a4}	s_{a5}	s_{b1}	s_{b2}	s_{b3}	s_{b4}	s_{b5}
0.25	0.21	0.98	1.4	1.4	0.21	0.48

https://doi.org/10.1017/S1759078726102955 Published online by Cambridge University Press

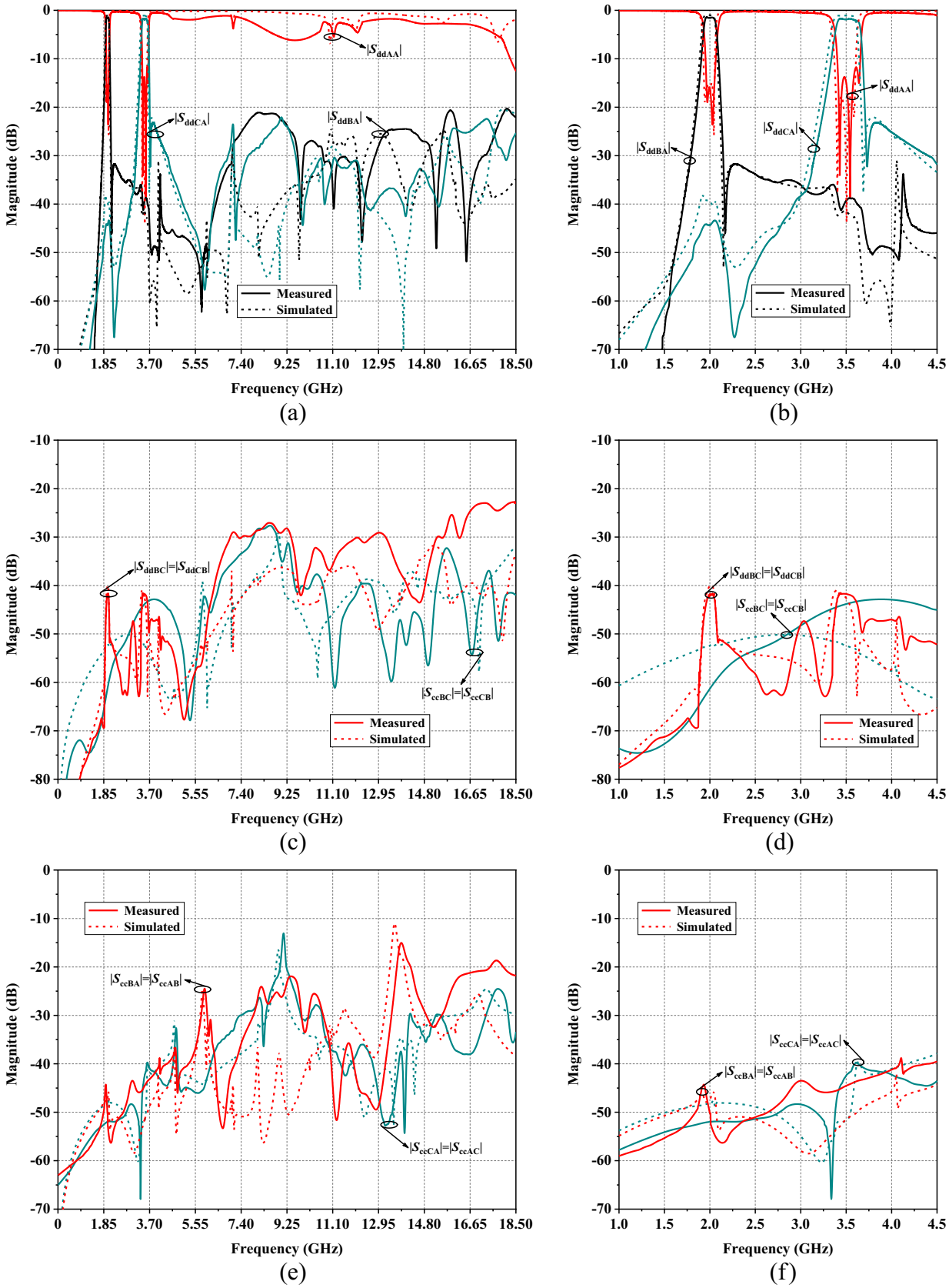


Figure 14. The simulated and measured mixed *S*-parameters. (a) Wideband DM frequency responses. (b) Details of the DM frequency response. (c) Wideband DM isolation and CM isolation. (d) Details of DM isolation and CM isolation. (e) Wideband CM frequency responses. (f) Details of the CM frequency response.

https://doi.org/10.1017/S1759078726102955 Published online by Cambridge University Press

Table 2. Performance comparisons with previous works

References	Center frequency (GHz)	Insertion loss (dB)	Balanced circuit	In-band DM isolation (dB)	In-band CM suppression (dB)	CM suppression level	DM stopband suppression level	Circuit size ($\lambda_g \times \lambda_g$)
[5]	1.94/2.50	0.46/0.50	No	35.0	-	-	>25 dB, ≈ 2.1f_L	0.64 × 0.56
[8]	2.45/5.50	1.67/1.58	No	25.8	-	-	>18 dB, ≈ 2.9f_L	0.22 × 0.16
[9]	2.05/2.45	1.13/1.35	No	20.0	-	-	>20 dB, 4.1f_L	0.33 × 0.21
[12]	2.41/3.61	1.46/2.15	No	38.0	-	-	>20 dB, ≈ 2.1f_L	0.66 × 0.15
[15]	2.59/5.41	2.73/3.68	Yes	40.0	30.0	>20 dB, ≈ 3.2f_L	>20 dB, ≈ 2.9f_L	0.55 × 0.39
[17]	2.45/5.05	1.20/1.60	Yes	39.0	34.0	-	-	0.24 × 0.14
[21]	2.20/2.63	1.06/1.09	Yes	38.0	23.0	-	-	0.61 × 0.34
[22]	2.47/3.48	1.12/1.45	Yes	30.0	51.0	>20 dB, ≈ 2.2f_L	>20 dB, ≈ 2.0f_L	≈ 0.25 × 0.22
[23]	1.47/2.19	0.94/2.20	Yes	40.0	39.1	>20 dB, ≈ 1.9f_L	>20 dB, ≈ 1.8f_L	≈ 0.39 × 0.12
[24]	2.73/3.10	1.19/1.55	Yes	17.3	38.6	-	>10 dB, ≈ 1.3f_L	0.66 × 0.44
[25]	2.40/2.60	1.50/1.60	Yes	40.0	40.0	>20 dB, ≈ 2.9f_L	>20 dB, ≈ 2.9f_L	0.33 × 0.11
[27]	2.51/3.57	1.14/1.21	Yes	35.0	49.1	>20 dB, ≈ 2.5f_L	>20 dB, 3.3f_L	-
	2.49/2.98	1.15/1.54	Yes	33.0	47.3	>30 dB, ≈ 4.0f_L	>20 dB, 3.7f_L	-
This work	**2.01/3.54**	**1.55/1.81**	**Yes**	**41.5**	**39.6**	**>20 dB, 6.8f_L**	**>20 dB, 9.2f_L**	**0.47 × 0.44**

thoroughly analyzed. A microstrip prototype was designed and fabricated based on this method. The measured results demonstrate that the balanced diplexer features excellent CM suppression, a wide stopband, and high isolation. Therefore, the proposed balanced diplexer has a good potential to be applied to dual-channel two-way balanced communication systems [24].

Acknowledgment. This work was supported by the National Natural Science Foundation of China (No. 61871417), the Natural Science Foundation of Liaoning Province (No. 2025-MSLH-097), the Basic Research Project of the Department of Education of Liaoning Province for Universities (No. LJ212410151023), the Liaoning Revitalization Talents Program (No. XLYC2007024), and the Fundamental Research Funds for the Central Universities (No. 3132025252).

Competing Interests. The authors report no conflict of interest.

References

1. **Yang T, Chi P-L and Itoh T** (2010) High isolation and compact diplexer using the hybrid resonators. *IEEE Microwave and Wireless Components Letters* **20**, 551–553. https://doi.org/10.1109/LMWC.2010.2052793
2. **Peng HS and Chiang YC** (2015) Microstrip diplexer constructed with new types of dual-mode ring filters. *IEEE Microwave and Wireless Components Letters* **25**(1), 7–9.
3. **Zhang ZC, Wong SW, Lin JY, Liu H, Zhu L and He Y** (2019) Design of multistate diplexers on uniform- and stepped-impedance stub-loaded resonators. *IEEE Transactions on Microwave Theory & Techniques* **67**(4), 1452–1460.
4. **Xiao JK, Zhu M, Li Y, Tian L and Ma JG** (2015) High selective microstrip bandpass filter and diplexer with mixed electromagnetic coupling. *IEEE Microwave and Wireless Components Letters* **25**(12), 781–783.
5. **Xue YM, Yang L, Xu JX, Zhao XL and Zhang XY** (2020) Wideband diplexer with narrow channel spacing using hybrid bandpass-bandstop structures. *IEEE Access* **8**, 137783–137788.
6. **Chen CF, Tseng BH, Su BY, Li XL, Wang GY and Li JJ** (2018) "Compact and high isolation microstrip six-channel diplexer using multi-mode stepped-impedance resonators," *2018 Asia-Pacific Microwave Conference (APMC)*, Kyoto, Japan. pp. 16–18.
7. **Roshani S and Roshani S** (2018) Design of a very compact and sharp bandpass diplexer with bended lines for GSM and LTE applications. *AEU-International Journal of Electronics and Communications* **99**, 354–360.
8. **Wu Y, Hao L, Wang W and Yang Y** (2022) Miniaturized and low insertion loss diplexer using novel inter-digital capacitors and microstrip section inductors. *IEEE Transactions on Circuits and Systems II: Express Briefs* **69**(11), 4303–4307.
9. **Xu JX, Zhan WL, Li HY and Zhang XY** (2021) Switchable diplexer based on coupling control. *IEEE Transactions on Circuits and Systems II: Express Briefs* **68**(1), 166–170.
10. **Chuang ML and Wu MT** (2011) Microstrip diplexer design using common T-Shaped resonator. *IEEE Microwave and Wireless Components Letters* **21**(11), 583–585.
11. **Guan X, Yang F, Liu H and Zhu L** (2014) Compact and high-isolation diplexer using dual-mode stub-loaded resonators. *IEEE Microwave and Wireless Components Letters* **24**(6), 385–387.
12. **Xiao JK, Zhang M and Ma JG** (2018) A compact and high-isolated multiresonator-coupled diplexer. *IEEE Microwave and Wireless Components Letters* **28**(11), 999–1001.
13. **Gómez-García R, Yang L and Munoz-Ferreras JM** (2020) Balanced quasi-elliptic-type combline diplexer with multiextracted-pole junction/output sections. *IEEE Microwave and Wireless Components Letters* **30**(6), 569–572.
14. **Song K, Yao J, Chen Y, Zhou Y, Zhu Y and Fan Y** (2020) Balanced diplexer based on substrate integrated waveguide dual-mode resonator. *IEEE Transactions on Microwave Theory & Techniques* **68**(12), 5279–5287.
15. **Chen CM, Chang SJ, Yang CF and Chen CY** (2015) A simple and effective method for designing frequency adjustable balun diplexer with high common-mode suppression. *IEEE Microwave and Wireless Components Letters* **25**(7), 433–435.

16. **Li WT, Zhang HR, Chai XJ, Mou JC, Hei YQ and Shi XW** (2023) Novel unbalanced-to-balanced quad-channel diplexer with controllable bandwidth and high isolation. *IEEE Transactions on Circuits and Systems II: Express Briefs* **70**(4), 1281–1285.
17. **Tian H, Liu H, Zheng S and Zuo T** (2023) Compact filtering balun-diplexer using coupled-line-loaded hairpin ring resonator. *IEEE Transactions on Circuits and Systems II: Express Briefs* **70**(3), 989–993.
18. **Zhou Y, Deng HW and Zhao Y** (2014) Compact balanced-to-balanced microstrip diplexer with high isolation and common-mode suppression. *IEEE Microwave and Wireless Components Letters* **24**(3), 143–145.
19. **Wei F, Liu WS, Wang JX and Zhao XB** (2023) Design of a novel balanced-to-balanced dual-band diplexing power divider. *IEEE Transactions on Circuits and Systems II: Express Briefs* **70**(2), 516–520.
20. **Zhao S, Wang Z, Gao M, Liu H and Fang S** (2024) Planar wideband balanced-to-balanced microstrip diplexer with reflectionless characteristics. *AEU-International Journal of Electronics and Communications* **177**, 155201.
21. **Zhang C, Zhu L and Li Y** (2018) Compact microstrip balanced-to-balanced diplexer using stub-loaded dual-mode resonators. *IEICE Electronics Express* **15**(5), 1–6.
22. **Song Y, Wen P, Liu H, Wang Y and Geng L** (2019) Design of compact balanced-to-balanced diplexer using dual-mode CRLH resonator for RFID and 5G applications. *IEEE Journal of Radio Frequency Identification* **3**(3), 143–148.
23. **Fernández-Prieto A, Lujambio A, Martín F, Martel J, Medina F and Boix RR** (2018) Compact balanced-to-balanced diplexer based on split-ring resonators balanced bandpass filters. *IEEE Microwave and Wireless Components Letters* **28**(3), 218–220.
24. **Wei F, Cheng XY, Liu YX and Shi XW** (2020) Balanced-to-balanced diplexer and quadruplexer with high selectivity and wide CM suppression. *IEEE Transactions on Circuits and Systems II: Express Briefs* **67**(11), 2467–2471.
25. **Deng H, Zhang T, Liu F, Xu T and Chen X** (2017) High isolation and common-mode suppression balanced-to-balanced microstrip diplexer with mixed coupling. *IEICE Electronics Express* **14**(24), 1–10.
26. **Liu H, Wang S, Sun M, Song Z and Tian H** (2024) Wide stopband and high isolation balanced diplexer using asymmetric hairpin ring resonator aided by grey wolf algorithm. *IEEE Transactions on Circuits and Systems II: Express Briefs* **71**(6), 2931–2935.
27. **Fernández-Prieto A, Lujambio A, Martel J, Medina F, Martín F and Boix RR** (2018) Balanced-to-balanced microstrip diplexer based on magnetically coupled resonators. *IEEE Access* **6**, 18536–18547.
28. **Eisenstant WR, Stengel B and Thompson BM**. (2006) *Microwave Differential Circuit Design Using Mixed-Mode S-Parameters*. Boston, MA: Artech House.
29. **Kuo JT and Shih E** (2003) Microstrip stepped impedance resonator bandpass filter with an extended optimal rejection bandwidth. *IEEE Transactions on Microwave Theory & Techniques* **51**(5), 1554–1559.
30. **Kuo JT and Lin HP** (2009) Dual-band bandpass filter with improved performance in extended upper rejection band. *IEEE Transactions on Microwave Theory & Techniques* **57**(4), 824–829.
31. **Hong JS and Lancaster MJ** (2001) *Microstrip Filters for RF/Microwave Applications* New York, NY, USA. *John Wiley & Sons*.



Changqing Geng received the B.Eng. degree in communication engineering from Dalian Minzu University, China, in 2023. He is currently working toward the M.Eng degree in communication engineering at Dalian Maritime University (DMU). His current research interests include balanced components and diplexers.



Zhongbao Wang received the Ph.D. degree in communication and information systems from DMU, China, in 2012. He is currently a Full Professor with the School of Information Science and Technology, DMU. From 2014 to 2018, he was a Postdoctoral Fellow with Beijing University of Posts and Telecommunications, China. From 2019 to 2020, he was a Visiting Scholar with National University of Singapore, Singapore. He has authored more than 150 journal papers. He is currently serving as a Technical Reviewer for the IEEE Trans. on Circuits and Systems, MTT, MWTL, MOTL, and so on. His current research interests include balanced RF components and filtering antennas.



Dehao Zhao received the Ph.D. degree in electronic science and technology from Beijing Institute of Technology, China, in 2024. He is currently a Lecturer with the School of Information Science and Technology, DMU. He current research interests include multifunctional microwave devices and spatio-temporal modulation technology.



Hongmei Liu received the Ph.D. degree in communication and information systems from DMU, China, in 2016. She is currently a Full Professor with the School of Information Science and Technology, DMU. Her current research interests include passive microwave circuits, reconfigurable RF components, and CP microwave antennas.



Shaojun Fang received the Ph.D. degree in communication and information systems from DMU, China, in 2001. Since 1982, he has been at DMU, where he is currently the Head Professor with the School of Information Science and Technology. He has authored or co-authored four books and over 120 journal and conference papers. His recent research interests include passive RF components and antennas.

https://doi.org/10.1017/S1759078726102955 Published online by Cambridge University Press